Mechanical Systems and Signal Processing (2000) **14**(6), 923–944
doi:10.1006/mssp.2000.1303, available online at http://www.idealibrary.com on IDEAL®

SELECTION AND UPDATING OF PARAMETERS FOR AN ALUMINIUM SPACE-FRAME MODEL

J. E. MOTTERSHEAD AND C. MARES

Department of Engineering, Mechanical Engineering Division, The University of Liverpool, U.K.

M. I. FRISWELL

Department of Mechanical Engineering, The University of Wales Swansea, U.K.

AND

S. JAMES

Department of Engineering, Mechanical Engineering Division, The University of Liverpool, U.K.

(Received 2 September 1999, accepted 9 March 2000)

A three-storey aluminium space frame is modelled using beam elements with unrepresentative rigid joints. Five model-updating experiments are carried out using different sets of updating parameters. All of them are shown to produce improved predictions, even for modified configurations of the frame. The set of parameters that on average produces the best results is also considered to provide a physical improvement to the modelling of the joints.

1. INTRODUCTION

An important aspect of finite element model updating [1, 2] is the choice of updating parameters. As a general rule, sensitive parameters should be chosen to converge the model predictions upon physical test results by a small parameter adjustment. However, the adjustment of the most sensitive parameters cannot always be justified by engineering understanding of the structure and the test carried out on it. Thus, uncertainty in the model should be located and parameterised sensitively to the predictions. Subspace selection methods [3, 4] may be applied to choose sensitive parameters and minimise the updating residual. In many cases, such as joints, the location of the uncertainty is not in dispute but there are many ways to parameterise joints [5, 6] some of which are sensitive and others insensitive.

Finite element model updating can generally be expressed as an ill-conditioned system of over-determined equations in the updating parameters. Regularisation by a minimum-norm constraint can often be applied effectively on a trial and error basis. More complicated side-constraints that embody some physical understanding not represented in the finite element model have been applied using formalised regularisation techniques [7]. Apart from the regularisation parameter, weights may be applied to the two systems of equations. In the Bayesian approach [8] the weights are related to the inverse covariances of the measurements and parameters, but the statistical data needed are not available. The authors' preferred approach is to use the weights to reinforce engineering understanding by stimulating convergence and preventing drift in the updated parameters. This can result in dissimilar weights being applied to parameters and measurements that seem to be equally uncertain. We remarked previously however that the sensitivity of the predictions to

different parameters can show large differences. Only if the updating equations are linear in the parameters, such as in the substructure parameters method [9], can normalisation of the parameters be carried out. Otherwise, it is the usual practice to non-dimensionalise the change in each parameter by dividing by its initial value. So, generally the parameters are adjusted by amounts that may differ by orders of magnitude. Consequently, to achieve a uniform convergence to many measurements and similar parameter adjustments one would expect to apply an irregular system of weights. The weights should be regarded as legitimate control parameters with which to influence the result in the direction of engineering understanding.

In this article, many candidate parameters are considered for updating the finite element model of a three-storey aluminium space frame. It is demonstrated that several different combinations of parameters can lead to acceptable convergence of the results. Amongst the chosen parameter sets there is one that provides a reasonable explanation of the initial deviation between the measurements and the finite element predictions. Convergence is achieved with acceptable adjustment of the parameters and higher damping in one mode is explained. The space frame is then reconfigured, both physically and in the updated model and good agreement is obtained.

2. THE ALUMINIUM SPACE FRAME

The three-storey aluminium frame was built using the Meroform $M12$ construction system consisting of 22 mm aluminium tubes connected by standard Meroform aluminium nodes. The complete structure is shown in Fig. 1 with electromagnetic shakers located at the first-floor level. The Meroform components are shown in more detail in Fig. 2. Each tube is fitted with a screwed end connector which when tightened into the node also clamps the tube by means of an internal compression fitting.

The length of all the horizontal and vertical tube-members between the centre of the joints is 707 mm. Two opposing vertical sides of the frame are stiffened by diagonal spars which cross in the centre of each storey when viewed from one side. This has the effect of separating the bending modes into two families in the x and y directions. It should be remarked that in both directions bending occurs independently of any twisting deformations. The twisting modes occur in two families too. These are characterised by shearing of the unstiffened/stiffened sides when viewed from above for the family with the lower/higher frequencies, respectively. The nodes at the base of the frame were clamped to a heavy steel table.

2.1. MODAL TESTING

The 'wire-frame' model illustrated in Fig. 3 shows the measurement points to be at each of the Meroform nodes. In an initial experiment the structure was excited by two electromagnetic shakers supplied with independent sequences of random noise at nodes 3 and 18 in a direction making an angle of 45° with the x- and y-axis as shown in Fig. 1. The vibration response was measured using 16 data collection channels from accelerometers on the structure. Measurements taken at nodes 2, 7, 12 and 17 showed negligibly small levels of vibration at the base. In a subsequent test hammer excitation was applied at the top of the frame (at node 20) at 45° in the plane x–y. Natural frequencies and mode shapes were extracted from the measured frequency response functions by using a time-domain multi-degree-of-freedom curve-fitting procedure from the LMS CADA-X system. The measured natural frequencies are given in Table 1 and examples of the mode shapes are illustrated in Fig. 4.

The shaker test showed a mode at 3.81 Hz which was attributed to 'nodding' of the shaker (and reaction mass) on the stinger, and was not present in the hammer-test results.

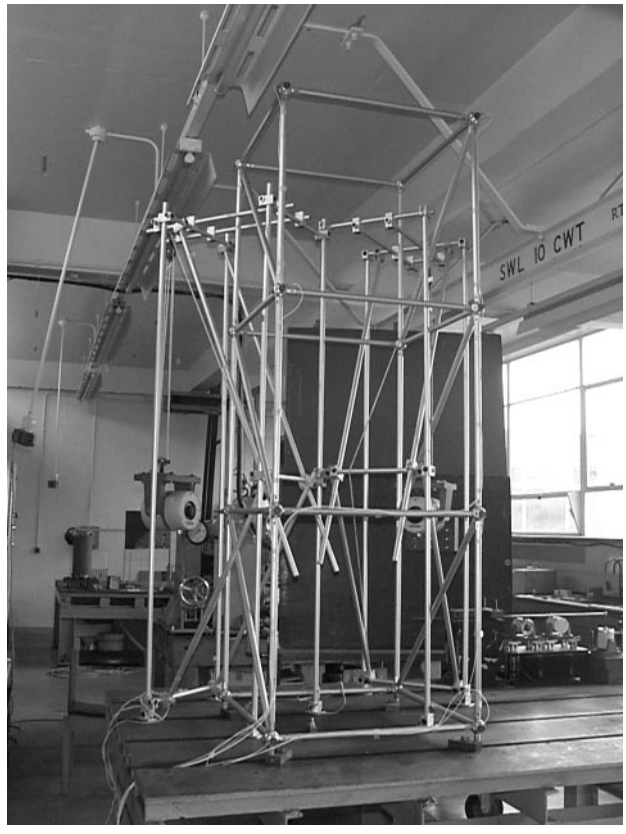

Figure 1. Aluminium space frame structure.

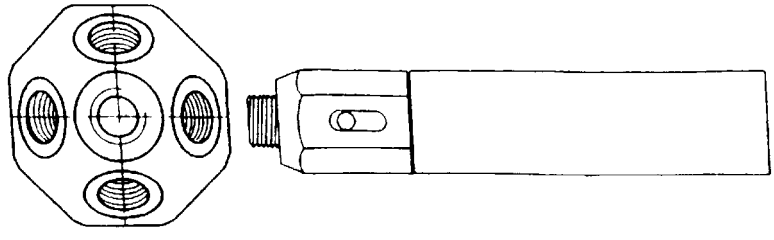

Figure 2. Meroform components.

The CADA-X system uses a stability plot [10] to determine the system poles, and in the shaker test a mode was indicated at 51.4 Hz without a definite sharp peak appearing in the frequency response curves. It was in fact the first bending mode in the x-direction. The hammer test revealed a clear peak at 51.2 Hz which was more heavily damped than the other modes. Frequency response plots obtained from the two tests are given in Figs. 5 and 6.

2.2. FINITE ELEMENT MODEL

A finite element model was assembled from 140 cubic Euler–Bernoulli beams. Four beam elements were used to model each tube over the complete length between two Meroform

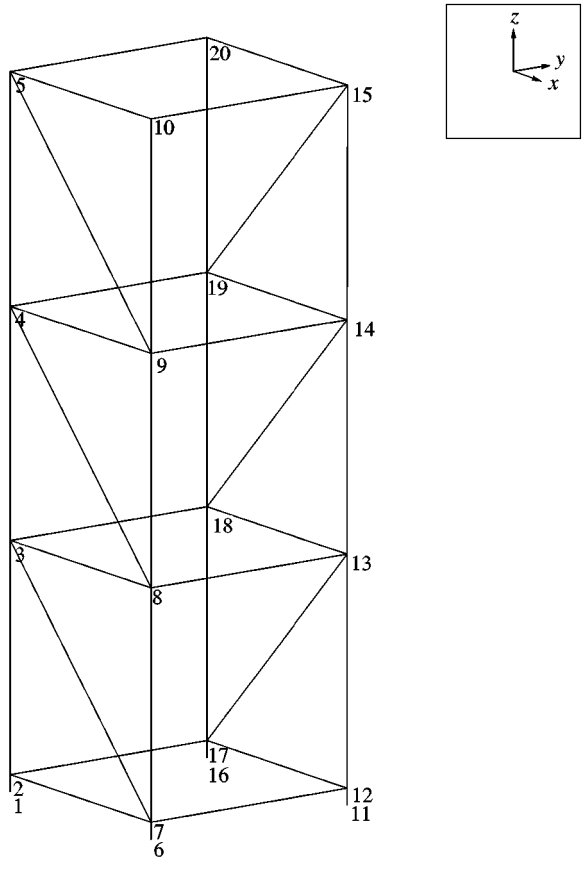

Figure 3. Modal analysis wire-frame model.

nodes and four further beam-elements were added to represent the fixing of the frame to the table. The model consisted of a total of 708 degrees-of-freedom. At the ends of the tubes there are stiff connectors which screw into the nodes, and these together with the nodes themselves were considered to be perfectly rigid. The element stiffness matrix for a beam in bending in the x–y plane, having a flexible length l separated by a rigid portion of length a from the first node can be written as

$$\boldsymbol{k} = \frac{EI_x}{l^3}\begin{bmatrix} 12 & (12a+6l) & -12 & 6l \\ (12a+6l) & (12a^2+12al+4l^2) & -(12a+6l) & (6al+2l^2) \\ -12 & -(12a+6l) & 12 & -6l \\ 6l & (6al+2l^2) & -6l & 4l^2 \end{bmatrix} \tag{1}$$

and the corresponding element mass matrix is

$$\boldsymbol{m} = \frac{\rho Al}{420}\begin{bmatrix} 156 & (156a+22l) & 54 & -13l \\ (156a+22l) & (156a^2+44al+4l^2) & (54a+13l) & -(13al+3l^2) \\ 54 & (54a+13l) & 156 & -22l \\ -13l & -(13al+3l^2) & -22l & 4l^2 \end{bmatrix}. \tag{2}$$

TABLE 1

Measured natural frequencies (Hz)

Mode	Shaker test	Hammer test	% Critical damping
Shaker-nodding mode	3.81	—	2.45
Bending *y*-direction	6.39	6.05	0.192
Bending *y*-direction	20.34	19.96	0.179
Shear *y*-direction	23.1	22.84	0.174
Shear *y*-direction	32.71	32.48	0.194
Bending *y*-direction	35.48	35.28	0.157
Torsion	42.80	42.68	0.215
Bending *x*-direction	51.38	51.18	2.143
Shear *x*-direction	60.83	60.71	0.643
Local bending	94.82	94.74	0.087
Local bending	100.44	99.96	0.169

The natural frequencies determined from the model are given in Table 2, together with the results of the hammer test, and a selection of the computed mode shapes are shown in Fig. 7. The greatest discrepancy between the measured and predicted natural frequencies is around 15% and occurs at the first bending mode in the *x*-direction and the first bending mode in the *y*-direction. The errors in the predicted natural frequencies are all positive which is consistent with the assumption of an over-stiff model caused by the rigid joints. The diagonal MAC terms were all better than 96% with very small off-diagonal terms.

In an attempt to reconcile the two sets of natural frequencies (before carrying out model updating) the shaker–stinger systems were each modelled with two beam elements and lumped masses and inertias. This resulted in the appearance of an additional natural frequency at 3.97 Hz corresponding to the measured value of 3.81 Hz from the shaker test. Otherwise the natural frequencies were unchanged. This (together with the results from the hammer test) confirmed that the stinger was providing bending isolation across the frequency range of the test. The finite element model is seen to be consistently stiffer than the physical structure and this was attributed to the rigid joints in the finite element model which fail to represent the flexibility of the beam-end connectors and the Meroform nodes.

3. PARAMETERS FOR MODEL UPDATING

It is possible to imagine many different parameterisations for updating the finite element model of the aluminium space frame. Perhaps the simplest approach is to parameterise substructure mass and stiffness matrices with a scalar multiplier as was advocated by Natke [9]. Although this method can be applied to a known erroneous substructure, it is unlikely to produce an updated model that is improved physically because it is unable to separate the error, that might for instance be present in a dimension across a structural member, from a multiplier that affects every term in the substructure stiffness (or mass) matrix. In a previous study Mottershead and James [11] updated the aluminium space frame using two updating parameters, the mass of the beam-end connector (denoted m_l) and the first bending eigenvalue of the element stiffness matrix immediately next to a joint. Whilst the study [11] resulted in good convergence of the finite element prediction on measured natural frequencies there remained serious doubts about the physical validity of the updated model. This

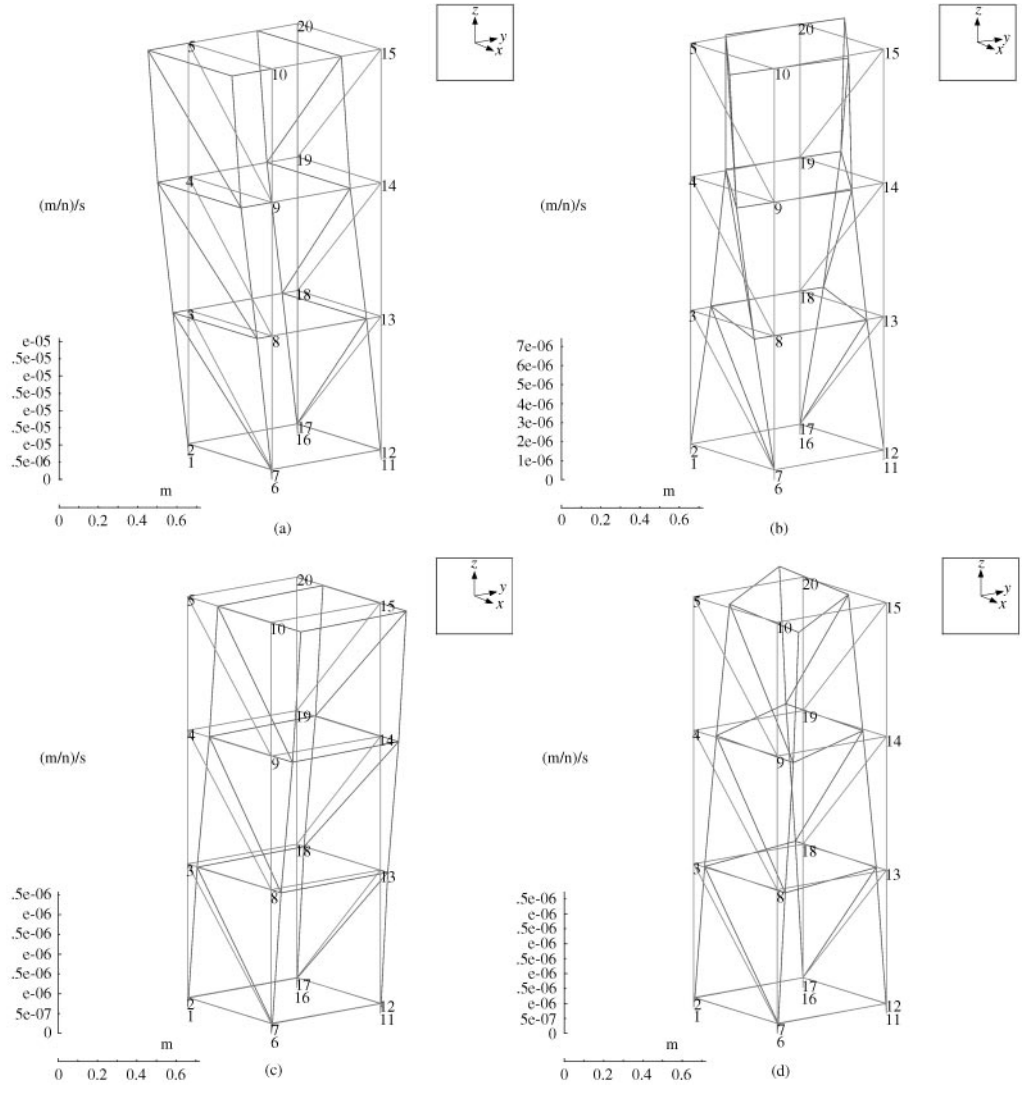

Figure 4. Experimental modes. (a) 1st mode. (b) 3rd mode. (c) 7th mode. (d) 8th mode.

was because the different elements of the space frame (the tubular spars, the Meroform nodes, and the beam-end connectors) had all been weighed, and the parameter m_l was considered to be well defined. In addition, it was found subsequently that the outside diameter of the tubes had been incorrectly specified at 20 mm.

Gladwell and Ahmadian [12] and Ahmadian *et al.* [13] showed how an element stiffness matrix can be adjusted by modifications to its eigenvalues and eigenvectors. In the case of a 12-degree-of-freedom beam/bar/torsion element with free ends there will be two bending eigenvalues in each of the two principal directions, an eigenvalue for extension/compression, a torsional eigenvalue and six rigid-body eigenvalues. The eigenvalue decomposition of a modified stiffness matrix can be expressed as

$$\boldsymbol{k} = \boldsymbol{\Psi}_0 \, \boldsymbol{\kappa} \boldsymbol{\Psi}_0^T \tag{3}$$

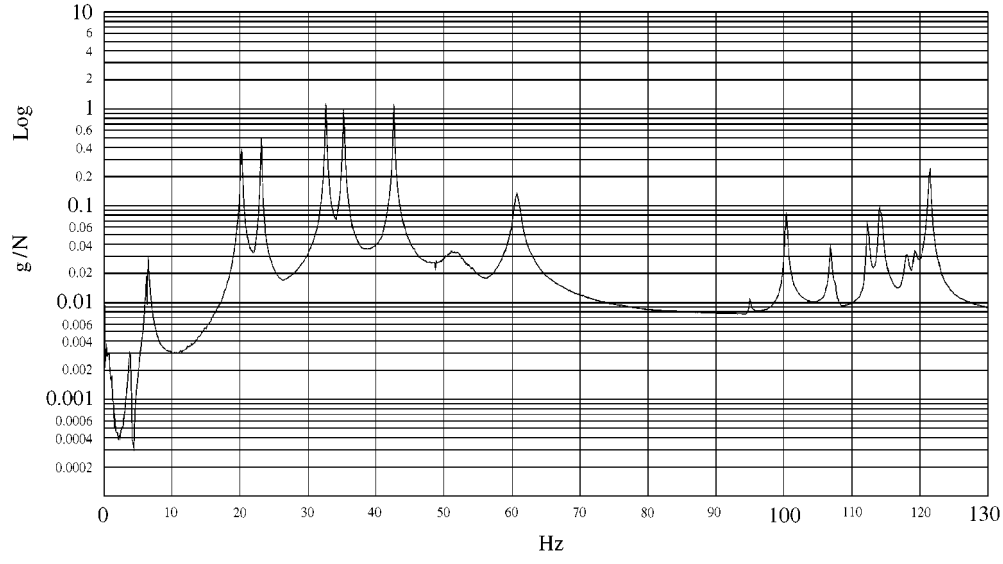

Figure 5. FRF plot—shaker test.

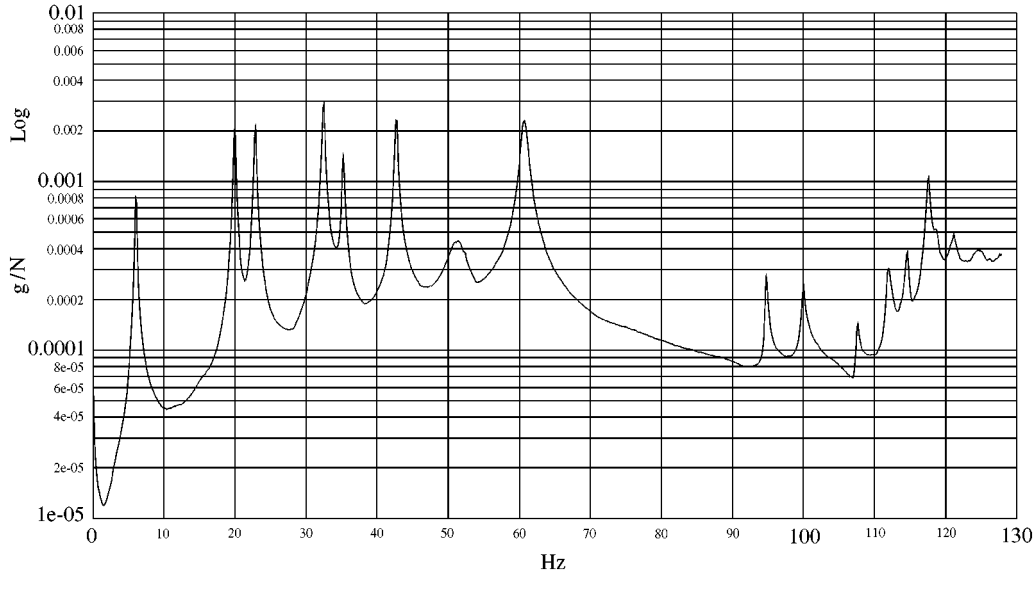

Figure 6. FRF plot—hammer test.

where

$$\boldsymbol{\kappa} = \boldsymbol{S}^T \boldsymbol{Q} \boldsymbol{S} \tag{4}$$

and the modes of the original stiffness, $\boldsymbol{\Psi}_0$, are related to the modified modes, $\boldsymbol{\Psi}$, by

$$\boldsymbol{\Psi}_0 = \boldsymbol{\Psi} \boldsymbol{S} \tag{5}$$

TABLE 2

Finite element predictions (Hz)

Mode	Experiment	Finite element	Error (%)
Bending *y*-direction	6.05	6.94	14.68
Bending *y*-direction	19.96	22.39	12.18
Shear *y*-direction	22.84	25.07	9.75
Shear *y*-direction	32.48	35.62	9.66
Bending *y*-direction	35.28	39.46	11.84
Torsion	42.68	46.93	9.96
Bending *x*-direction	51.18	58.70	14.68
Shear *x*-direction	60.71	66.01	8.72
Local bending	94.74	98.26	3.70
Local bending	99.96	104.44	4.48

so that $\boldsymbol{S}^T = \boldsymbol{S}^{-1}$ when the columns of $\boldsymbol{\Psi}$ (and separately the columns of $\boldsymbol{\Psi}_0$) are orthogonal. The matrix $\boldsymbol{Q} = diag(q_i)$, $i = 1, \ldots, n_s$, contains the non-zero eigenvalues of the original stiffness matrix and $\boldsymbol{\Psi}_0 = \{\boldsymbol{\psi}_{01}, \ldots, \boldsymbol{\psi}_{0n_s}\}$, where n_s denotes the number of strain modes. The most general approach is to take all the elements of $\boldsymbol{\kappa}$ as updating parameters in which case both the eigenvalues and eigenvectors of the stiffness matrix will be adjusted. By imposing the constraint $\boldsymbol{S} = \boldsymbol{I}$ it is possible to adjust the eigenvalues without making any changes to the original eigenvectors. Mottershead and James [11] updated the first bending eigenvalue, q_1^b, of the part-rigid/part-flexible element used to model the tubular spars next to the joint. The resulting stiffness adjustment occurs entirely in the flexible part of the element and not in the Meroform node and end-connector which contain an unmodelled flexibility which is thought to be responsible for the discrepancy between the measurements and finite element predictions.

Mottershead *et al.* [5] updated two welded joints by using offset parameters. In the particular case of the aluminium frame structure the offset is represented by the term denoted '*a*' in equations (1) and (2). Of course, the stiffness matrices responsible for bending in the *x*–*z* plane, extension/compression and torsion (not given in this article) all have a similar rigid portion, *a*, at a joint-end. It is conceivable that there should be a different offset in extension, a_{ext}, to bending in the plane *x*–*y*, a_{xy}. If the distance between the Meroform nodes is to remain unchanged then a reduction to the rigid length, *a*, must be accompanied by equal extension to the flexible length, *l*. In addition to the mass, element eigenvalue/eigenvector and offset parameters, the wall thickness of the tube, *t*, was included as a global updating parameter. Although it is not possible to measure the wall thickness without damaging one of the spars it was considered reasonable that a small variation in *t* (from its nominal 1 mm value) might be expected.

3.1. SENSITIVITY ANALYSIS

In this study the finite element model is updated by using eigenvalue sensitivities determined according to

$$\frac{\partial \lambda_i}{\partial \theta_j} = \boldsymbol{\varphi}_i^T \left(\frac{\partial \boldsymbol{K}}{\partial \theta_j} - \lambda_i \frac{\partial \boldsymbol{M}}{\partial \theta_j} \right) \boldsymbol{\varphi}_i \tag{6}$$

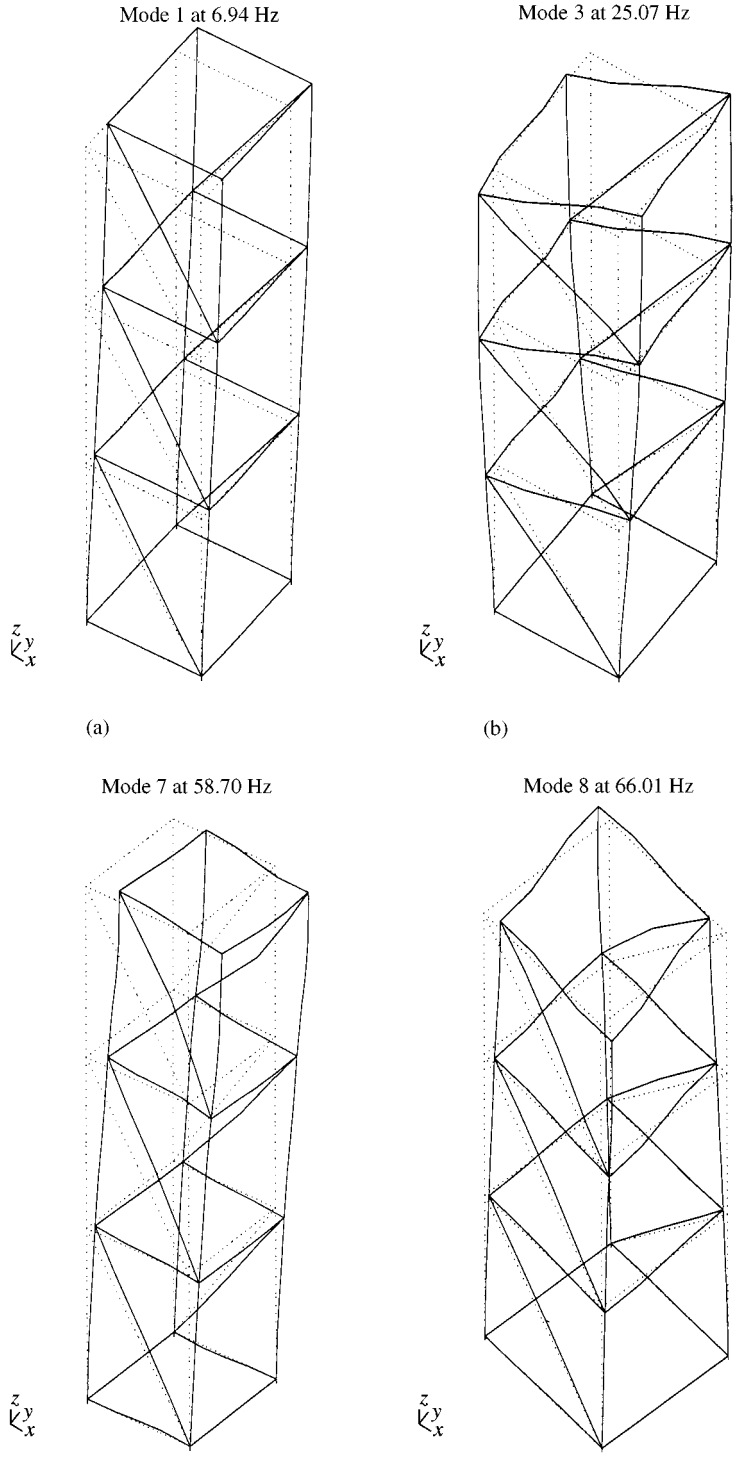

Figure 7. Finite element modes.

where λ_i and $\boldsymbol{\varphi}_i$ represent the ith eigenvalue and eigenvector, respectively, and θ_j is an updating parameter. When θ_j is a substructure parameter [9] the derivatives $\partial \boldsymbol{K}/\partial\theta_j$ and $\partial \boldsymbol{M}/\partial\theta_j$ are identically the substructure stiffness and mass matrices. For a stiffness-eigenvalue parameter,

$$\frac{\partial \boldsymbol{K}}{\partial q_j} = \boldsymbol{\psi}_{oj}\boldsymbol{\psi}_{oj}^T. \tag{7}$$

The derivative of $\boldsymbol{K}$ with respect to the offset parameter, a, was calculated approximately using the formula

$$\frac{\partial \boldsymbol{K}}{\partial a} = \frac{\boldsymbol{K}(a + \Delta a) - \boldsymbol{K}(a)}{\Delta a}. \tag{8}$$

The eigenvalue sensitivities to many different parameters are given in Table 3. The parameters are normalised in the form $(\delta\theta/\theta_o)$ and in that case the sensitivities become $((\partial\lambda/\partial\theta)\theta_o)$. The first three parameters, $\theta_V\theta_H$ and θ_D, are scalar multipliers applied to those vertical, horizontal and diagonal elements, respectively, having one end at a Meroform node. Parameter m_g represents the mass of such a node. The first 10 eigenvalues, $\lambda_1, \ldots, \lambda_{10}$, are all less sensitive to m_g than to m_l. The parameters q^t and q^{ext} are the torsional and extension/compression element stiffness eigenvalues and are identical to κ_{11} and κ_{66}, respectively. The torsional sensitivities are insignificant until the ninth eigenvalue is reached. However, the seventh and eighth modes are seen to be very sensitive to extension and compression. The two modes denoted by λ_7 and λ_8 are both dominated by in-plane bending of the two stiffened sides of the frame as shown in Figs. 4(c) and 4(d).

Almost all the modes, but especially λ_7 and λ_8, are strongly sensitive to the wall thickness t. Of course, when t is adjusted all the elements are changed and not just those at the joints (as with the other parameters). Therefore, it is expected that the eigenvalues will be sensitive to t. The influence of the offset parameter a is about as strong as t, but when the extension/compression offset a_{ext} is separated from the bending and torsion it becomes clear that the sensitivity $\partial\lambda_7/\partial a$ is dominated by $\partial\lambda_7/\partial a_{\text{ext}}$. The eighth mode is also very sensitive to a_{ext}. This result is not unexpected because we already observed the strong sensitivity of λ_7 and λ_8 to $q^{\text{ext}}(=\kappa_{66})$. However a_{ext} seems to be a better parameter than q^{ext} because it represents an adjustment at the joint (the rigid part of the element) whereas q^{ext} is a spring constant for the flexible part. The eigenvalues λ_7 and λ_8 are the first x-direction bending and shear modes and there is no significant x-bending in any of the other modes. Thus, when a is separated into the two bending planes z–x and z–y it is seen that λ_7 and λ_8 are sensitive to a_{zx} and the other modes are all insensitive. Conversely, λ_7 and λ_8 are insensitive and the other modes are sensitive to a_{zy}.

4. MODEL UPDATING EXPERIMENTS

Five separate model updating experiments were carried out using different parameters as follows: (1) m_l and q_1^b as in the previous article [11], (2)θ_V, θ_H and θ_D substructure multipliers, (3) all elements $\kappa_{11}, \kappa_{12}, \ldots, \kappa_{66}$ of the generic element matrix $\boldsymbol{\kappa}$, (4) t and a, and t and a_{zx} in two stages, and (5) t, a and a_{ext}.

The finite element model was updated by minimisation of an objective function having the form

$$J = (\delta\lambda - \boldsymbol{S}\delta\theta)^T \boldsymbol{W}_\lambda(\delta\lambda - \boldsymbol{S}\delta\theta) + (\theta - \theta_0)^T \boldsymbol{W}_\theta(\theta - \theta_0) \tag{9}$$

TABLE 3

Table of sensitivities

Par	λ_1	λ_2	λ_3	λ_4	λ_5	λ_6	λ_7	λ_8	λ_9	λ_{10}
ϑ_V	615.69	8703.21	2521.69	13729.88	39914.50	45907.52	38893.93	40213.07	22450.30	61687.13
ϑ_H	875.53	6506.08	15498.09	25478.95	7811.33	25336.73	6358.63	32376.15	75664.72	56236.32
ϑ_D	52.44	671.72	1372.51	1656.63	2567.02	1463.40	15217.76	16774.07	14625.71	20340.09
m_g	−264.47	−2761.53	−3744.48	−7739.99	−8358.78	−12293.83	−18853.86	−24947.54	−999.74	−1934.14
m_l	−939.26	−10196.18	−13773.43	−28071.71	−33923.15	−49325.01	−64936.24	−85973.71	−3298.03	−7892.22
q^t	2.15	38.16	227.40	1291.18	152.26	1606.71	32.74	337.64	7501.30	13241.20
q_1^b	1480.87	15246.78	16967.14	38026.33	48464.34	68672.48	1943.07	28483.58	96727.86	114239.13
q_2^b	52.86	529.18	591.32	1297.56	1625.30	2332.50	254.70	1114.83	7790.24	10046.85
q^{ext}	5.74	45.96	1567.48	189.63	26.00	50.97	58236.57	59346.40	523.05	597.19
κ_{11}	2.15	38.16	227.40	1291.18	152.26	1606.71	32.74	337.64	7501.30	13241.20
κ_{22}	577.98	5667.59	6754.44	12720.86	15066.94	18266.78	1235.78	11150.22	36998.03	40793.24
κ_{33}	902.89	9579.19	10212.71	25305.46	33397.40	50405.69	707.30	17333.36	59729.82	73445.89
κ_{44}	44.69	449.78	202.10	739.78	1329.71	1639.68	92.09	354.69	3493.11	4537.15
κ_{55}	8.16	79.40	389.23	557.78	295.59	692.81	162.61	760.14	4297.13	5509.70
κ_{66}	5.74	45.96	1567.48	189.63	26.00	50.97	58236.57	59346.40	523.05	597.19
t	936.03	10251.18	15086.62	30080.01	34725.99	51900.99	78802.19	102348.30	−2670.54	803.44
a	987.68	10093.03	12093.12	25716.82	31825.40	45880.45	28805.15	46685.40	39896.55	54913.73
a_{ext}	28.55	293.43	907.95	843.29	850.07	1254.73	22042.78	23175.88	278.03	396.58
a_{zx}	0.00	0.03	15.86	2.38	0.05	1.07	2861.56	3970.62	0.99	3.59
a_{zy}	383.07	5258.57	1362.18	8306.75	23834.58	27229.68	19.41	169.41	7971.22	18112.86

Note: ϑ, *substructure parameters for vertical, horizontal and diagonal groups of elements*; m_g, *node mass*; m_l, *beam end mass*; q, *eigenvalues of the generic element*; κ, *diagonal elements of the generic element*; t, *thickness*; a, *offset*.

where $\delta\lambda$ is a vector of small changes in structural eigenvalues, $\boldsymbol{S}$ is the matrix of eigenvalue sensitivities, $(\theta - \theta_0)$ is the vector of parameter deviations from the initial values necessary to eliminate the discrepancy $\delta\lambda$, and $\delta\theta$ is the incremental parameter change. $\boldsymbol{W}_\lambda$ and $\boldsymbol{W}_\theta$ are positive-definite weighting matrices and the terms in these matrices must be selected on the basis of engineering understanding to produce acceptable parameters θ. Generally, large terms in $\boldsymbol{W}_\lambda$ will tend to stimulate convergence whilst large terms in $\boldsymbol{W}_\theta$ have the effect of restraining the parameters to a small deviation from the initial finite element model.

In the five experiments, the eigenvalue weights were mostly set as

$$\boldsymbol{W}_\lambda = diag(500,\ 500,\ 20,\ 10,\ 8,\ 5,\ 4,\ 7,\ 1.2,\ 1)$$

so that the eigenvalues with lower numerical values were given high weights to compensate for the strong effect the higher eigenvalues would have on the results $\delta\theta$ by virtue of the large numbers associated with them. The seventh and eighth-eigenvalues were consistently reluctant to converge and λ_8 was given a weighting slightly larger than the general trend of numbers in $\boldsymbol{W}_\lambda$. The converged natural frequencies (after eight updating iterations) are shown in Table 4. Similar convergence is obtained from all five experiments, though experiments (3) and (5) appear to be slightly better than the others, and the greatest discrepancy in every case but one occurs in the seventh natural frequency. This is the same mode that had been difficult to excite in the modal tests.

The parameter weights in experiment (1) were

$$w_{m_l} = 5 \times 10^{-6}, \qquad w_{q_b^1} = 5 \times 10^{-4}.$$

This combination of weights results in the updated parameters shown (in non-dimensional form) in Table 5, and their convergence at each of the eight iterations is shown in Fig. 8.

In experiment (2) equal weights were applied to the three substructure parameters θ_V, θ_H and θ_D. Thus

$$\boldsymbol{W}_\theta = diag(1,1,1) \times 10^{-5}.$$

The updated parameters are given in Table 6 and a convergence graph is shown in Fig. 9.

When using the fully populated generic element matrix, $\boldsymbol{\kappa}$, the parameter weights in experiment (3) were set according to

$$w_{\kappa_{ij}} = 5 \times 10^{-6}, \quad i = j$$

$$w_{\kappa_{ij}} = 1 \times 10^{-10}, \quad i \neq j.$$

This arrangement would allow the off-diagonal terms of $\boldsymbol{\kappa}$ to deviate quite freely from their original zero values. However, the off-diagonals remained small and the updated diagonal terms are given in Table 7. The convergence plot is shown in Fig. 10. The parameters that changed most were $\kappa_{66}(= q^t)$ and $\boldsymbol{\kappa}_{22}(= q_1^b)$.

The updating was carried out in two steps in experiment (4). Firstly, eight iterations were completed to adjust the parameters t and a and in the second step eight further iterations were done to update t and a_{zx}. The purpose of the second step can be seen from Table 3 to be the convergence of the seventh and eighth modes which had failed to converge at the end of the first step. In the second step the eigenvalue weights were changed to

$$w_{\lambda_7} = 40, \quad w_{\lambda_8} = 40.$$

The parameter weights were,

$$w_t = 5 \times 10^{-4}, \quad w_a = 1 \times 10^{-4}$$

TABLE 4

Natural frequencies and errors (%) *after updating in eight iterations*; 1—*updating using* m_l *and* q_1^b; 2—*substructure multipliers*; 3—*all* κ*'s of the generic element stiffness matrix*; 4—*correction in two stages*: *first t and a and then t and* a_{zx}; 5—*t*, *a and* a_{ext}

	Frequency (Hz)									
Expt.	f_1	f_2	f_3	f_4	f_5	f_6	f_7	f_8	f_9	f_{10}
1	6.21(2.66)	19.98(0.11)	22.29(−2.40)	31.58(−2.79)	34.99(−0.83)	41.51(−2.74)	54.02(5.54)	60.23(−0.79)	97.30(2.70)	103.25(3.29)
2	6.32(4.48)	20.08(0.60)	23.37(2.33)	32.71(0.70)	34.41(−2.48)	41.96(−1.70)	53.07(3.69)	60.24(−0.77)	94.88(0.14)	99.48(−0.48)
3	6.21(2.62)	20.08(0.62)	22.43(−1.79)	32.06(−1.30)	35.43(0.42)	42.47(−0.97)	53.28(4.11)	59.76(−1.57)	94.63(−0.12)	100.51(0.55)
4	6.18(2.05)	19.92(−0.23)	22.22(−2.73)	31.48(−3.10)	34.93(−1.00)	41.39(−3.03)	54.19(5.88)	60.31(−0.66)	96.68(2.04)	102.35(2.40)
5	6.18(2.15)	19.98(0.10)	22.34(−2.19)	31.78(−2.16)	35.14(−0.39)	41.75(−2.19)	53.73(4.98)	60.09(−1.03)	96.24(1.58)	101.88(1.92)

TABLE 5

Updated parameters (1)

m_l	q_1^b
1.3755	0.9366

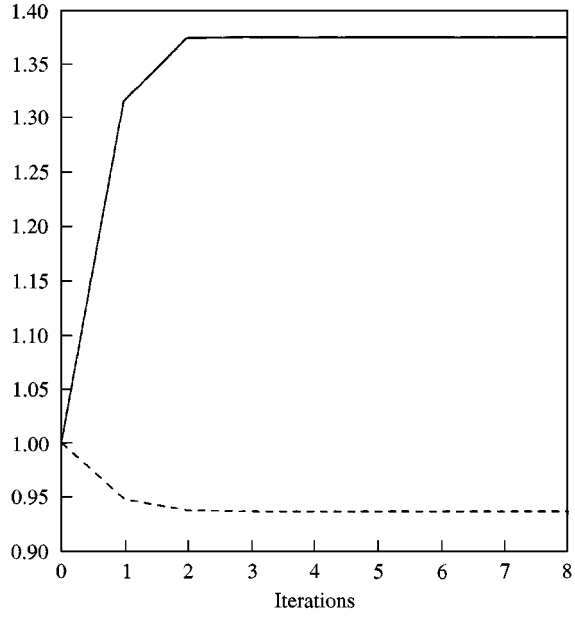

Figure 8. Parameter convergence plot (1). -- first bending eigenvalues; —— beam end mass.

TABLE 6

Updated parameters (2)

ϑ_V	ϑ_H	ϑ_D
0.7111	0.9044	0.5217

in step 1 and

$$w_t = 1 \times 10^{-2}, \quad w_{a_{zx}} = 1 \times 10^{-5}$$

in step 2. This has the effect of restraining the modification to t in the second part of the experiment. The updated parameters are shown in Table 8 and Figs. 11 and 12.

In experiment (5) the updating parameters were t, a_{ext} and a where in this case a represents all offsets except the extensional one. The weights were

$$w_t = 1 \times 10^{-2}, \quad w_{a_{\text{ext}}} = 5 \times 10^{-5}, \quad w_a = 1 \times 10^{-5}$$

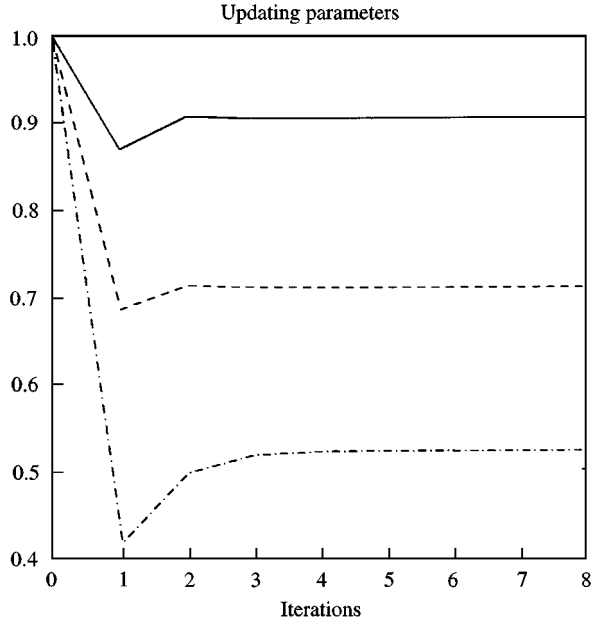

Figure 9. Parameter convergence plot (2). – – verticals; —— horizontals; –·–·– diagonals.

TABLE 7
Updated parameters (3)

κ_{11}	κ_{22}	κ_{33}	κ_{44}	κ_{55}	κ_{66}
0.9612	0.7019	0.7985	0.9448	0.9976	0.6722

and

$$w_{\lambda_7} = 40, \quad w_{\lambda_8} = 40.$$

The updated parameters are given in Table 9 and their convergence is shown in Fig. 13.

5. DISCUSSION

The results shown in Table 4 indicate that good convergence of predictions on measured natural frequencies can be achieved using many different systems of updating parameters. The seventh mode had been the most difficult to excite in modal tests and was consistently the less well converged after eight updating iterations. This mode and the eighth, which required a larger weight to bring about convergence, are both characterised by in-plane bending of the two stiffened sides of the frame. This is likely to cause extension/compression in the diagonal spars. Evidence of this can be found in Table 3 where both λ_7 and λ_8 are found to be strongly sensitive to θ_D and a_{ext}. Of course, the presence of the diagonal spars will also give rise to significant extension/compression in the vertical and horizontal members, but in modes 1–6 there is very little sensitivity to the diagonals.

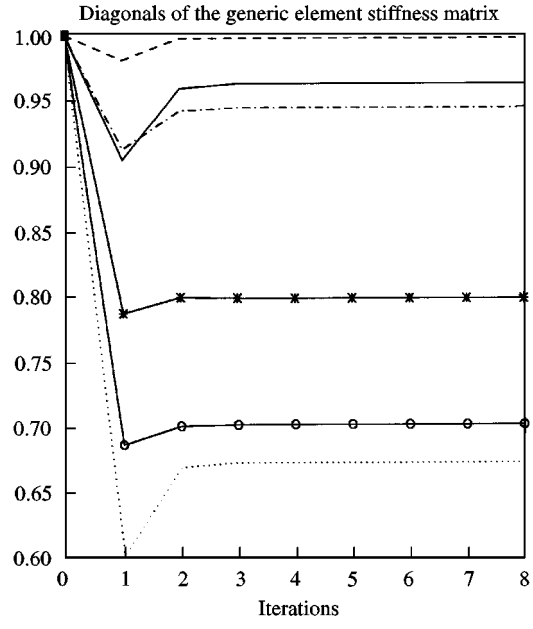

Figure 10. Parameter convergence plot (3). —— 1st; ○ 2nd; × 3rd; –·–·– 4th; – – 5th; ····· 6th.

TABLE 8

Updated parameters (4)

t	a	a_{zx}
0.8621	0.6872	0.2762

Experiment (1) results in a 38% increase in the mass of the beam-end connector which seems unrealistic as the masses of the components are well defined. However, the major adjustment occurs at the joints where the modelling error is considered to be located.

In Experiment (2) the substructure multipliers θ_V, θ_H and θ_D are modified by different amounts. Since the vertical, horizontal and diagonal elements are (nominally) identical there seems to be no physical reason which can be used to explain the different adjustments.

Adjusting the terms in the generic element matrix, $\boldsymbol{\kappa}$, results in experiment (3) in a significant modification to the term κ_{66} most associated with extension/compression and the first bending eigenvalues in the two principal directions κ_{22} and $\boldsymbol{\kappa}_{33}$. The off-diagonal terms take small values after updating which have the effect of modifying the eigenvectors of the element stiffness matrices at the joints. This means that the separation of the element into distinctly rigid and flexible parts does not apply in the updated model.

In experiment (4) the offset a_{zx} in the z–x plane of bending is reduced to a much greater extent than the other bending offsets. Whilst this can bring about a convergence of the predicted natural frequencies a modification of this kind cannot be explained physically because the spars should clearly have the same bending stiffness in all directions.

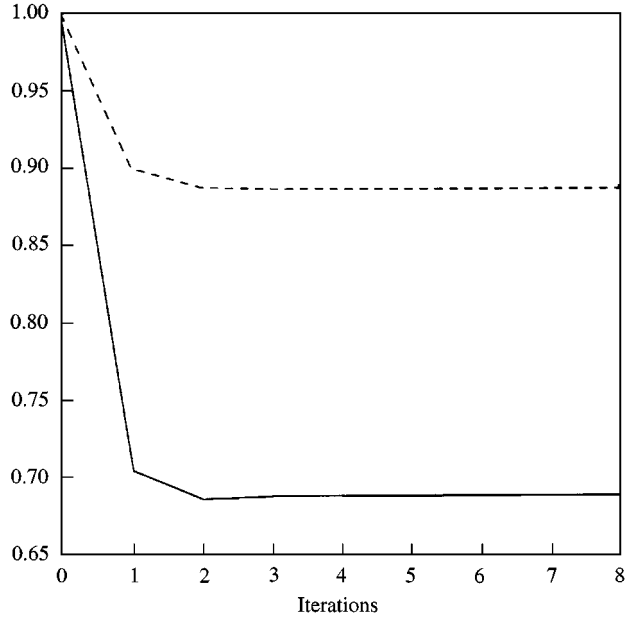

Figure 11. Parameter convergence plot (4)—first phase. -- t; —— a.

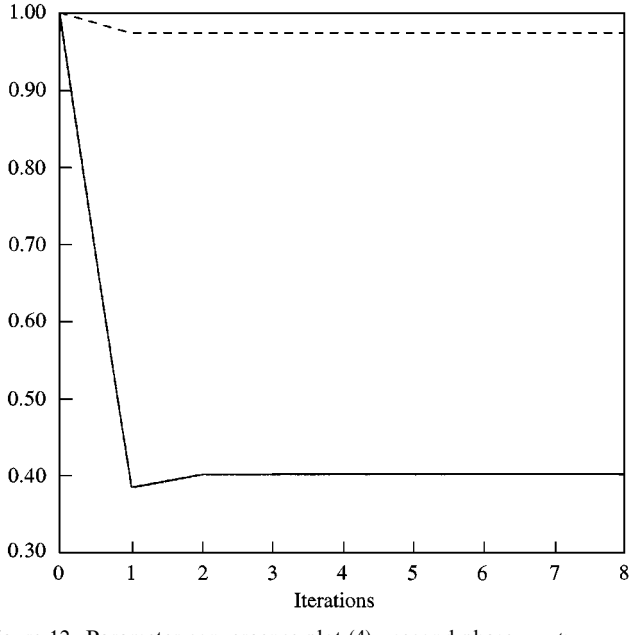

Figure 12. Parameter convergence plot (4)—second phase. -- t; —— a_{zx}.

TABLE 9

Updated parameters (5)

t	a	a_{ext}
0.9836	0.5693	0.0373

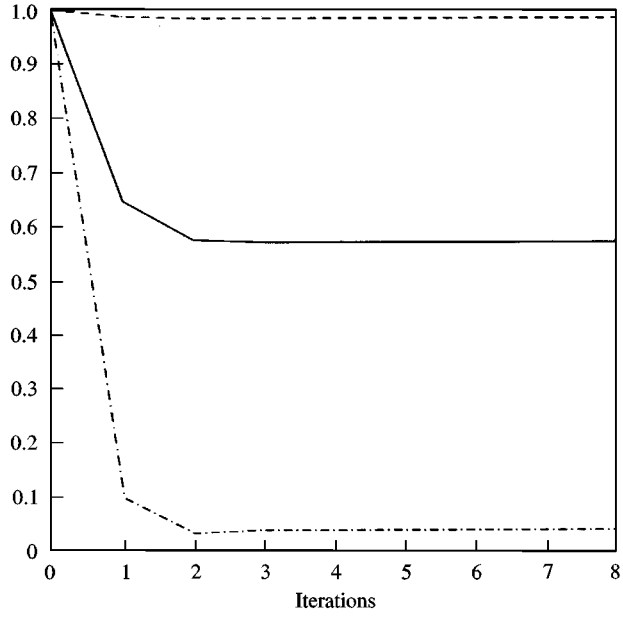

Figure 13. Parameter convergence plot (5). – – t; —— a_bending; – · – · – a_extension.

TABLE 10

Measured natural frequencies and finite element predictions for the second configuration

Mode	Experiment (Hz)	Finite element (Hz)	Error (%)
Bending y-direction	5.71	6.93	21.29
Bending y-direction	19.92	22.36	12.24
Shear y-direction	22.48	25.17	11.97
Shear y-direction	31.90	35.76	12.10
Bending y-direction	34.88	39.73	13.87
Torsion	42.31	47.29	11.75
Bending x-direction	51.61	58.65	13.64
Shear x-direction	60.91	66.07	8.64

In experiment (5) the extensional offset a_{ext} is separated from the bending and torsional offsets and both are updated together with the wall-thickness t. The results appear to be reasonably acceptable on physical grounds. Only slightly different results can be produced by using a different system of weights. In addition, the high damping shown in Table 1 for mode 7 might be due to friction (micro-slip) in the compression fitting that clamps the tube to its end-connector when the joints are tightened. It is noticeable from Table 1 that mode eight (which also shows in-plane bending of the stiffened sides of the frame and sensitivity to extension/compression) has a high damping level too, though not as high as mode seven.

5.1. DIFFERENT CONFIGURATIONS

The frame was physically re-constructed in two different configurations to test the quality of the updated models produced from the five experiments. The second and third

TABLE 11

Natural frequencies and errors (%) using the updated parameters for the second configuration FE model

Expt.	Frequency (Hz)							
	f_1	f_2	f_3	f_4	f_5	f_6	f_7	f_8
1	6.27(9.66)	20.06(0.69)	22.25(−1.02)	31.97(0.20)	35.96(3.07)	42.59(0.65)	53.95(4.53)	60.11(−1.32)
2	6.32(10.52)	20.06(0.71)	23.43(4.24)	32.79(2.78)	34.61(−0.78)	42.22(−0.22)	53.02(2.74)	60.29(−1.02)
3	6.22(8.78)	20.01(0.47)	22.49(0.05)	32.38(1.50)	36.28(4.00)	43.16(2.00)	53.21(3.09)	59.66(−2.06)
4	5.93(3.70)	18.88(−5.25)	22.08(−1.79)	30.52(−4.35)	32.75(−6.11)	39.28(−7.17)	54.36(5.32)	60.59(−0.52)
5	6.17(8.00)	19.94(0.12)	22.43(−0.22)	31.87(−0.09)	35.39(1.44)	42.03(−0.68)	53.69(4.02)	60.13(−1.29)

Note: 1—m_l *and* q_1^b; 2—*substructure multipliers*; 3—*all* κ*'s of the generic element stiffness matrix*; 4—*correction in two stages*: *first* t *and* a *and then* t *and* a_{zx}; 5—t, a *and* a_{ext}

TABLE 12

Measured natural frequencies and finite element predictions for the third configuration

Mode	Experiment (Hz)	Finite element (Hz)	Error (%)
Bending *y*-direction	6.07	6.94	14.33
Bending *y*-direction	19.54	21.93	12.23
Shear *y*-direction	29.60	32.25	8.95
Bending *y*-direction	33.70	37.84	12.28
Torsion	51.76	55.93	8.05
Bending *x*-direction	—	57.40	—
Local bending	94.57	95.67	1.16
Local bending	100.67	103.40	2.71

configurations differ from the original arrangement of the frame as follows: In the second configuration the direction of the diagonals between nodes 5 and 9, 4 and 8, and 3 and 7 were changed to 4 and 10, 3 and 9, and 2 and 8. Then, when looking on one side, all the diagonals are aligned in the same direction. In the third configuration, additional diagonal spars were introduced between nodes 4 and 14, and 8 and 18 at the first and second floor levels. The side-diagonals were returned to their original positions.

The experimental natural frequencies for the second configuration are compared to predictions from unmodified (not updated) finite elements in Table 10. The results obtained when using elements that had been updated in the previous five experiments are shown in Table 11. Significant improvements are obtained in all cases. The updated elements produced by experiment (5) reduced an error of 21% in the first mode to 8%.

For the third configuration the experimental and unmodified finite element results are shown in Table 12, and the results obtained by using elements updated by the five experiments are given in Table 13. In this configuration, two close modes at 55.93 and 57.4 Hz were found from the finite element analysis but only one of them could be found in the modal test. All five models built from updated elements give significantly improved results over the unmodified finite element model. The model that uses elements updated from experiment (5) gives excellent results that are even better than those obtained for the original configuration.

6. CONCLUSIONS

The convergence of finite element predictions on measured natural frequencies can be obtained by many different sets of updating parameters. The finite elements produced by different updating parameterisations can be assembled into models that represent a change in the configuration of the structure under test, and even then may show a marked improvement in the predictions.

Not all the parameter sets (that result in improved predictions) can be justified physically. In the case of the aluminium frame structure considerable understanding was achieved by carrying out the five updating experiments. In particular, it became clear that the seventh and eighth modes (in the original configuration) were strongly affected by extension and compression in the Meroform joints. The updating parameters used in experiment (5) are considered to provide a physical improvement over the original (unmodified) finite element model. The high level of damping in the seventh mode might be due to micro-slip in the compression fitting that clamps the tube to its end-connector when the joints are tightened.

TABLE 13

Natural frequencies and errors (%) using the updated parameters for the third configuration FE model

Expt.	Frequency (Hz)							
	f_1	f_2	f_3	f_4	f_5	f_6	f_7	f_8
1	6.27(3.27)	19.71(0.88)	28.74(−2.91)	34.36(1.95)	50.70(−2.05)	52.80(−)	92.76(−1.91)	96.58(−4.07)
2	6.26(3.21)	19.59(0.26)	29.68(0.26)	32.92(−2.31)	50.90(−1.67)	51.88(−)	89.48(−5.38)	94.48(−6.15)
3	6.22(2.42)	19.65(0.58)	29.00(−2.03)	34.57(2.57)	50.70(−2.04)	52.09(−)	91.23(−3.53)	94.68(−5.95)
4	5.94(−2.15)	18.51(−5.25)	28.00(−5.40)	31.16(−7.53)	50.85(−1.75)	53.23(−)	92.66(−2.02)	98.84(−1.82)
5	6.22(2.47)	19.65(0.56)	29.16(−1.50)	33.83(0.38)	52.49(1.41)	54.66(−)	93.17(−1.48)	99.05(−1.61)

Note: 1—m_l *and* q_1^b; 2—*substructure multipliers*; 3—*all* κ*'s of the generic element stiffness matrix*; 4—*correction in two stages*: *first t and a and then t and* a_{zx}; 5—*t*, *a*, *and* a_{ext}

ACKNOWLEDGEMENT

The research reported in this article is supported by EPSRC grant GR/M08622. Dr Friswell gratefully acknowledges the support of EPSRC through the award of an Advanced Fellowship.

REFERENCES

1. J. E. MOTTERSHEAD and M. I. FRISWELL 1993 *Journal of Sound and Vibration* **162**, 347–375. Model updating in structural dynamics: a survey.
2. M. I. FRISWELL and J. E. MOTTERSHEAD 1995 *Finite Element Model Updating in Structural Dynamics*. Dordrecht: Kluwer Academic Press.
3. G. LALLEMENT and J. PIRANDA 1990 *Proceedings of the* 8*th IMAC*, Orlando, Florida, 579–585. Localisation methods for parameter updating of finite element models in elastodynamics.
4. M. I. FRISWELL, J. E. MOTTERSHEAD and H. AHMADIAN 1998 *Transactions of the ASME, Journal of Vibration and Acoustics* **120**, 854–859. Combining subset selection and parameter constraints in model updating.
5. J. E. MOTTERSHEAD, M. I. FRISWELL, G. H. T. NG and J. A. BRANDON 1996 *Mechanical Systems and Signal Processing* **10**, 171–182. Geometric parameters for finite element model updating of joints and constraints.
6. H. AHMADIAN, J. E. MOTTERSHEAD and M. I. FRISWELL 1997 *Proceedings of the* 15*th IMAC*, Orlando, Florida, 3–6 February 1997, 142–146. Parameterisation and identification of a rubber seal.
7. H. AHMADIAN, J. E. MOTTERSHEAD and M. I. FRISWELL 1998 *Mechanical Systems and Signal Processing* **12**, 47–64. Regularisation methods for finite element model updating.
8. T. T. SOONG 1981 *Probabilistic Modelling and Analysis in Science and Engineering*. New York: John Wiley and Sons.
9. H. G. NATKE 1988 *Probabilistic Engineering Mechanics* **3**, 28–35. Updating computational models in the frequency domain based on measured data: a survey.
10. J. LEURIDAN, J. LIPKENS, H. VAN DER AUWERAER and F. LEMBREGHTS 1986 4*th IMAC*, Los Angeles, CA, 1568–1595. Global modal parameter estimation methods: an assessment of time vs frequency domain implementation.
11. J. E. MOTTERSHEAD and S. JAMES 1998 *Proceedings of the* 16*th IMAC*, Santa Barbara, CA, February 2–5, 8–11. Updating parameters for the model of a three-storey aluminium space frame.
12. G. M. L. GLADWELL and H. AHMADIAN 1996 *Mechanical Systems and Signal Processing* **9**, 601–614. Generic element matrices for finite element model updating.
13. H. AHMADIAN, G. M. L. GLADWELL and F. ISMAIL 1997 *Transactions of the ASME, Vibration and Acoustics* **119**, 37–45. Parameter selection strategies in finite element model updating.